

Article

Study of Nanometer-Sized Precipitation and Properties of Fire Resistant Hot-Rolled Steel

Zhenjia Xie ¹, Zhendong Song ², Kun Chen ¹, Minghong Jiang ¹, Ya Tao ², Xuemin Wang ¹ and Chengjia Shang ^{1,*}

¹ Collaborative Innovation Center of Steel Technology, University of Science and Technology Beijing, Beijing 100083, China; zjxie@ustb.edu.cn (Z.X.); chenkunqing@126.com (K.C.); 17801051733@163.com (M.J.); wxm@mater.ustb.edu.cn (X.W.)

² Technical Center of Inner Mongolia Baotou Steel Union Co., Ltd., Baotou 014010, China; szhd1982@126.com (Z.S.); Taoya2002@sina.com (Y.T.)

* Correspondence: cjshang@ustb.edu.cn; Tel.: +86-10-6233-4910

Received: 27 October 2019; Accepted: 13 November 2019; Published: 18 November 2019



Abstract: Nanometer-sized precipitated carbides in a low carbon Ti-V-Mo bearing steel were obtained through hot rolling and air cooling and were investigated by transmission electron microscopy (TEM). The nanometer-sized interphase-precipitated carbides have been found to exhibit an average diameter of $\sim 6.1 \pm 2.7$ nm, with an average spacing of $\sim 24\text{--}34$ nm. Yield strength of 578 ± 20 MPa and tensile strength of 813 ± 25 MPa were achieved with high elongation of $25.0 \pm 0.5\%$ at room temperature. The nanometer-sized precipitation exhibited high stability after annealing at high temperatures of 600 °C and 650 °C for 3 h. Average diameters of carbides were statistically measured to be $\sim 6.9 \pm 2.3$ nm and 8.4 ± 2.6 nm after tempering at high temperatures of 600 °C and 650 °C, respectively. The micro-hardness was $\sim 263\text{--}268$ HV0.1 after high temperature tempering, which was similar to the hot-rolled sample (273 HV0.1), and yield strength of 325 ± 13 MPa and 278 ± 4 MPa was achieved at elevated temperatures of 600 °C and 650 °C, respectively. The significant decrease of yield strength at 650 °C was attributed to the large decrease in shear modulus.

Keywords: interphase precipitation; high temperature strength; stability; low carbon; low alloy steel

1. Introduction

As reference a material, high-strength low-alloy (HSLA) steel is of great importance for construction materials. With buildings tending to be high-rise and large-scale, there is an increased demand in higher strength steel for consideration of self-weight reduction, green, and safety [1]. Moreover, fire-resistant performance of structural steel has gained more attention since the sudden collapse of the World Trade Center towers due to the 9/11 terrorist attack in 2001. Therefore, for the fire-resistant HSLA steel, the strictest requirement is that the yield strength at 600 °C should be guaranteed to be higher than two-thirds of the yield-strength value specified at room temperature [2]. However, strength of steel inevitably decreases at high temperature in fire. The rapid decrease in strength has been suggested to be attributed to thermal activation processes, including atomic diffusion, coarsening of precipitates, and dislocation recovery and annihilation [3].

In order to develop fire-resistant steel, plenty of studies have been carried out by researchers. Studies [4,5] suggested that Mo addition was an effective approach for achieving high strength at high temperature for low alloy steels. It was suggested that there was a strength increment of ~ 13.7 MPa per 0.1% Mo addition at 600 °C when the total Mo content was lower than 0.5% by solid-solution strengthening and bainite strengthening [6–8]. However, as an expensive alloying element, high-addition of Mo will greatly increase the cost. Therefore, an alternative method by

microalloying of Nb, V, and Ti and controlled accelerated cooling was introduced to low carbon low Mo steels for fire-resistant applications [1,9,10]. In this method, bainite strengthening was obtained by controlled accelerated cooling, and remained microalloying elements of Nb, V, and Ti in solid-solution precipitates as nanometer-sized MC-type carbides at elevated temperature in fire to provide high temperature strength. However, accelerated cooling process generates higher energy-consumption and water-pollution in comparison with a hot rolling process. In addition, the remaining microalloying elements in solid-solution waste resources.

Interphase precipitation strengthening is generally recognized as an effect and economic approach in developing high-strength low-alloy hot-rolled steels [11–14]. Previous published works have shown that the nanometer-sized interphase precipitated carbides could contribute 300–400 MPa to yield strength of hot-rolled steels [15,16]. The objective of the present work is to develop a high-strength low-alloy fire-resistant steel by introducing nanometer-sized interphase precipitation of microalloying element carbides. Transmission electron microscopy (TEM) characterization investigated the stability of interphase precipitated carbides including size, morphology, and distribution. Moreover, the effect of nanometer-sized interphase precipitated carbides on strength at elevated temperatures was discussed. The findings from the present study may provide an alternative approach for developing high-strength fire-resistant hot-rolled steels.

2. Experimental Material and Procedure

The chemical composition of the experimental steel based on low carbon, high titanium, and vanadium micro-alloying design is in weight percent (wt.%): 0.08C, 1.43Mn, 0.21Si, <1.0(Ni+Cr+Cu), 0.27Mo, <0.25(Nb+Ti+V). Low carbon and low manganese alloy design was good for weldability [17]. The combined addition of Ni, Cr, and Cu aimed to obtain good weather-resistant performance [18]. The steel was melted in a high frequency induction vacuum furnace (ZGIL0.1-200-2.5, Jinzhou, China) and cast into 25 kg ingot in a cylindrical shape with a diameter of ~120 mm. The ingot was re-heated to 1200 °C for homogenization, then hot rolled to a 20-mm thick plate through seven passes. The starting temperature of hot rolling was ~1020 °C and the finishing temperature was ~860 °C. During the entire hot rolling, a minimum reduction rate of 20% per pass was given. Lastly, the plate with a thickness of 20 mm was air cooled to an ambient temperature.

Tensile specimens in a dog-bone-shape with a gauge length of 50 mm and a diameter of 10 mm were prepared from the hot-rolled plate along the longitudinal direction. The tensile tests were conducted at room temperature and at elevated temperatures (600 °C and 650 °C), according to the Chinese standards GB/T228-2002 and GB/T4338-2015, respectively. Before high temperature tensile tests, tensile specimens were held at elevated temperatures for 3 h. Two samples were tested for each testing temperature and the average values were taken for the results of tensile tests. Specimens for microstructure examinations were cut from the edge of the tensile tested samples. The specimens for scanning electron microscopy (SEM) and microhardness tests were etched in 3% nital after mechanical grinding and polishing. SEM was performed using the TESCAN MIRA 3 LMH (Brno, Czech Republic) field-emission scanning electron microscope (FE-SEM). Vickers microhardness was measured at a load of 100 g. More than 30 measurements in ferrite were conducted for each sample. Samples obtained after annealing at 600 °C for 3 h and a uniform deformed section at 600 °C, respectively, were prepared for electron backscatter diffraction (EBSD) by metallographic mechanical polishing and electrolytic polishing. EBSD analysis was conducted using TESCAN MIRA 3 LMH FE-SEM equipped with an Oxford Symmetry EBSD detector at an acceleration voltage of 20 kV and a step size of 0.2 µm. EBSD data was post-processed by HKL CHANNEL 5 (Oxford, UK) flamenco software to acquire the necessary information. Thin foils with ~400 µm thickness were cut from the edge of samples after tensile tests at room temperature and elevated temperatures. Then, the thin foils were mechanically ground to ~60 µm thickness. Next, TEM disks (3 mm in diameter) in diameter were punched from the foils and twin-jet polished using an electrolyte consisting of 5% perchloric acid and 95% methanol at ~−20 °C. TEM observations were performed using FEI Tecnai F20 (Hillsboro, OR, USA) field-emission

transmission electron microscope (FE-TEM) and FEI Tecnai G20 (Hillsboro, OR, USA) transmission electron microscope both combined with an energy dispersive X-ray spectrometer (EDS) detector at 200 kV.

3. Results and Discussion

3.1. Tensile Properties

Tensile properties of the hot-rolled steel were measured at room temperature and elevated temperatures. The obtained results are summarized in Table 1. After hot-rolling, the experimental steel exhibited high yield strength of 578 ± 20 MPa, high tensile strength of 812 ± 25 MPa, and high elongation of $25.0 \pm 0.5\%$ at room temperature. After holding at $600\text{ }^{\circ}\text{C}$ for 3 h, the yield strength and tensile strength of the studied steel were 325 ± 13 MPa. It was found that the studied hot-rolled steel met two-thirds of 460 MPa grade yield strength for fire-resistant structural application. When further elevating the test temperature to $650\text{ }^{\circ}\text{C}$, the yield strength and tensile strength were further decreased to 278 ± 4 MPa.

Table 1. Tensile properties of the hot rolled steel at room temperature and elevated temperatures.

Testing Temperature	Yield Strength, MPa	Tensile Strength, MPa	Elongation, %
Room temperature	578 ± 20	812 ± 25	25.0 ± 0.5
$600\text{ }^{\circ}\text{C}$	325 ± 13	-	-
$650\text{ }^{\circ}\text{C}$	278 ± 4	-	-

3.2. Microstructure and Microhardness

Figure 1 presents the optical microstructure of the hot-rolled steel. It can be seen that multi-phase microstructure consisting of polygonal ferrite and bainite was obtained in the hot-rolled steel. By statistical analysis of more than 10 optical images, the volume fraction of ferrite and bainite was determined to be $\sim 84\%$ and $\sim 16\%$, respectively. The grain size of ferrite was not uniform and has been found to range from ~ 2 to $\sim 30\text{ }\mu\text{m}$. To study the grain size of ferrite, EBSD analysis was performed, and the obtained band contrast (BC) image is given in Figure 2a. In Figure 2a, grain boundaries with misorientation higher than 5° were highlighted by black lines. It was easy to find out polygonal ferrite and bainite due to their different morphologies. After getting rid of bainite manually, the ferrite grain size was determined using HKL CHANNEL 5 flamenco software. The obtained results are plotted in Figure 2b. It can be seen that wide range distribution of grain size was obtained. The majority of ferrite grains ranged from $2\text{--}10\text{ }\mu\text{m}$ with the peak at $\sim 4\text{ }\mu\text{m}$. A few ferrite grains had a size of $\sim 10\text{--}30\text{ }\mu\text{m}$ with a small peak at $\sim 13\text{ }\mu\text{m}$. During continuous air cooling, ferrite transformation took place continuously at different temperatures. The grain size of ferrite is related to the transformation temperature, which determines the carbon atom diffusivity and the austenite/ferrite grain boundary migration rate [19]. Based on this, the grain size of ferrite formed at high temperature should be larger than that formed at a low temperature [20]. However, ferrite grain size also depends on the density of nucleation sites. In this work, austenite grains were flattened after final rolling at $860\text{ }^{\circ}\text{C}$. During subsequent air cooling, high dense ferrite grains nucleated at austenite grain boundaries, grain corners, and deformation bands. These tiny ferrite grains were not coalesced during the following cooling, as reported in literature [21]. In the late period of air cooling, a few ferrite grains nucleated surrounding the tiny ferrite grains and grew into residual austenite, and the large size of ferrite grains was obtained. From the EBSD image in Figure 2a, it can be seen that large ferrite grains were mainly adjacent to bainite, which transformed from carbon-enriched residual austenite in the final stage of air cooling. This observation gives evidence to support that the later mechanism was the reason for the wide range distribution of grain sizes observed in the present work. Moreover, the hot deformation was helpful for refining ferrite grains by promoting the nucleation of ferrite by introducing crystal defects within parent grains [20], which resulted in a fine average grain size of $\sim 5.06 \pm 3.93\text{ }\mu\text{m}$ for ferrite.

Microstructure and microhardness for the studied steel after hot rolling and high temperature holding were investigated. The obtained results are presented in Figure 3. From Figure 3a–c, it can be seen that both SEM microstructure and microhardness were not changed clearly for the hot-rolled steel before and after holding at 600 °C and 650 °C for 3 h. The average Vickers microhardness of the hot-rolled steel was $HV0.1\ 276 \pm 10$. After holding at 600 °C and 650 °C for 3 h, the average Vickers microhardness of the studied steel decreased slightly to $HV0.1\ 268 \pm 12$ and $HV0.1\ 263 \pm 9$, respectively. It can be found that the ferrite obtained through hot-rolling presented high resistance to soften after high temperature holding.

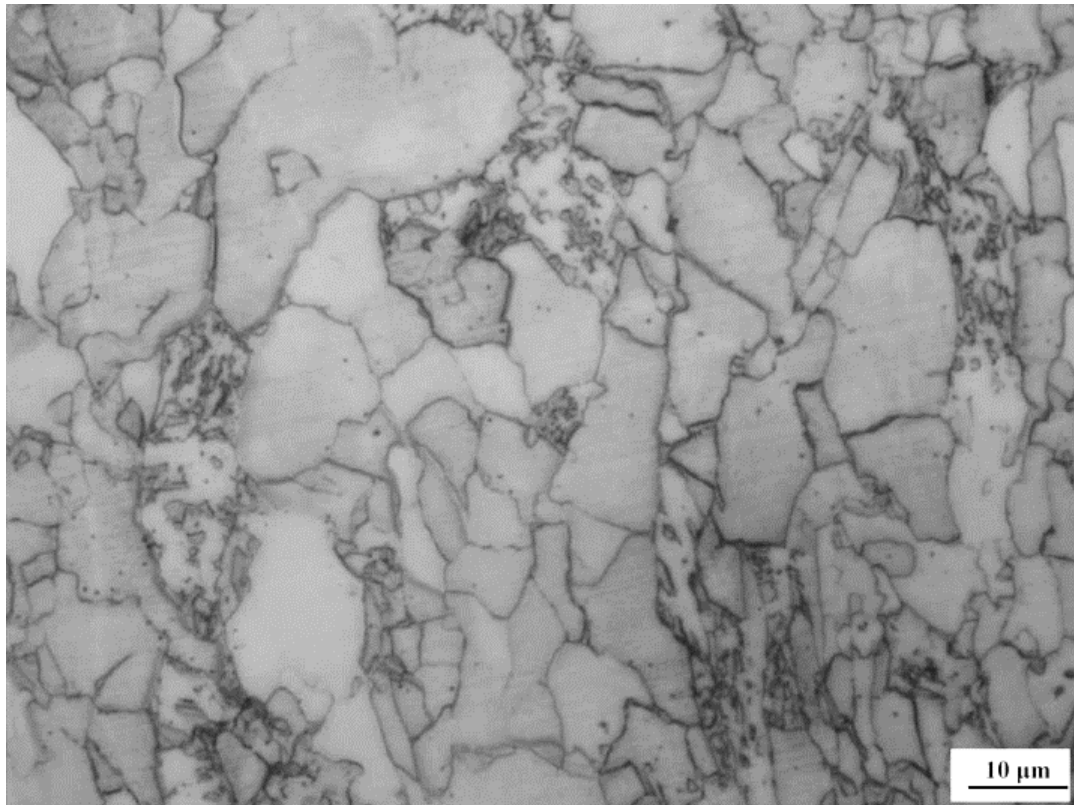
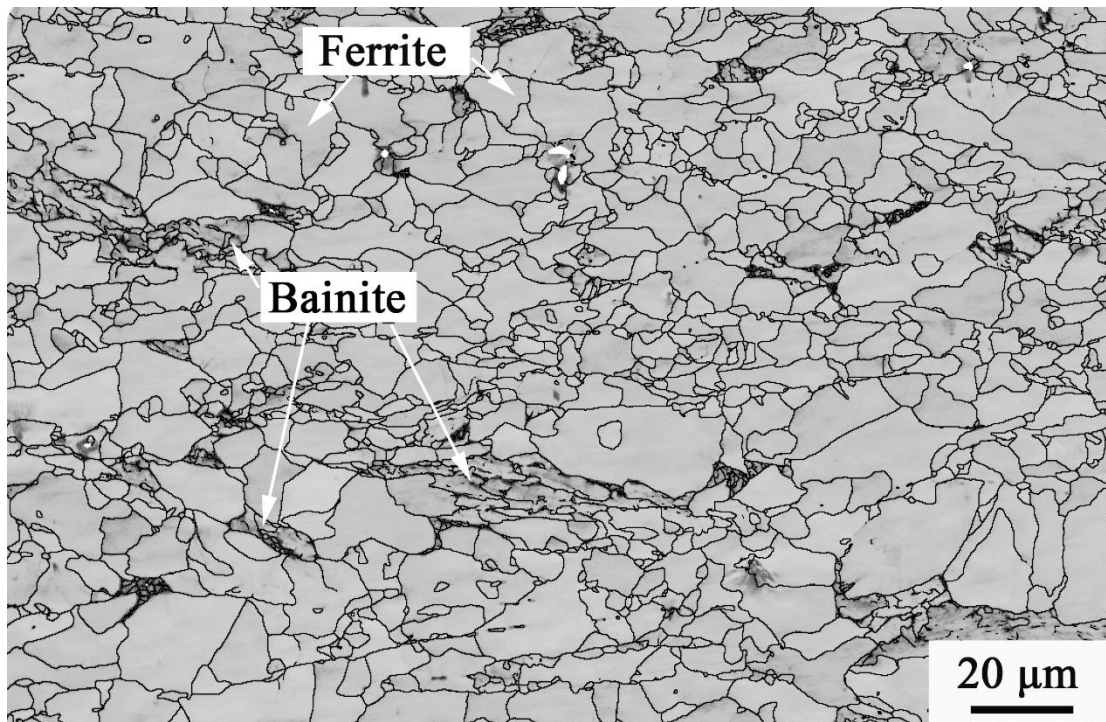
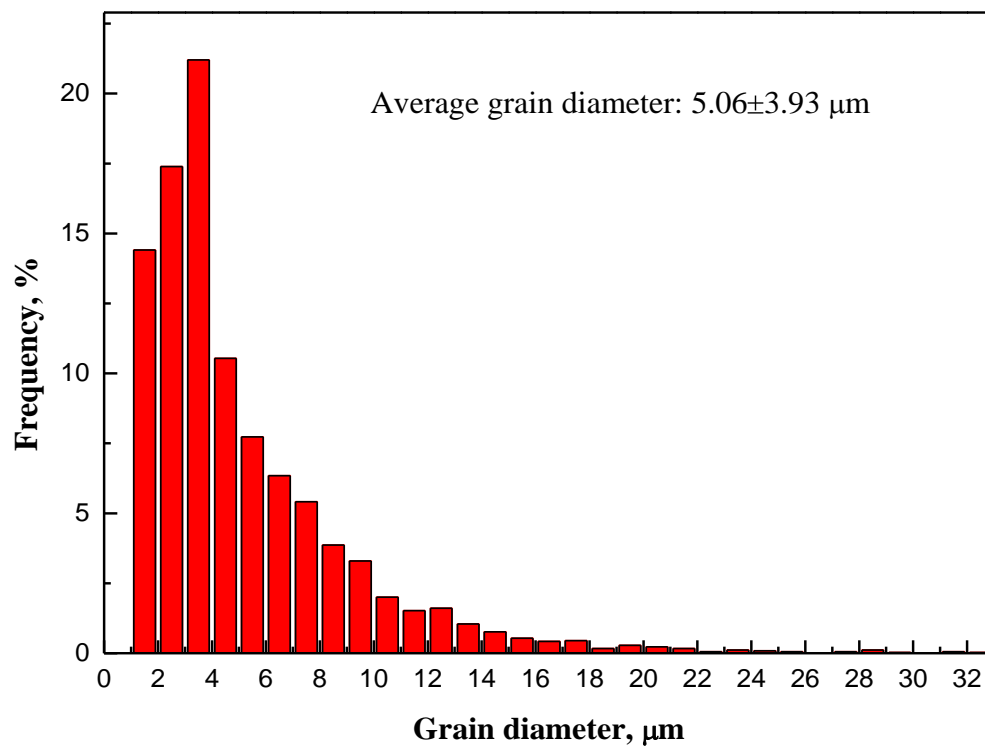


Figure 1. Optical microstructure of the hot-rolled experimental steel.



(a)



(b)

Figure 2. (a) EBSD image showing ferrite grains and bainitic microstructure. (b) The ferrite grain size distribution profile obtained from the EBSD image using HKL CHANNEL 5 flamenco software after getting rid of bainite manually.

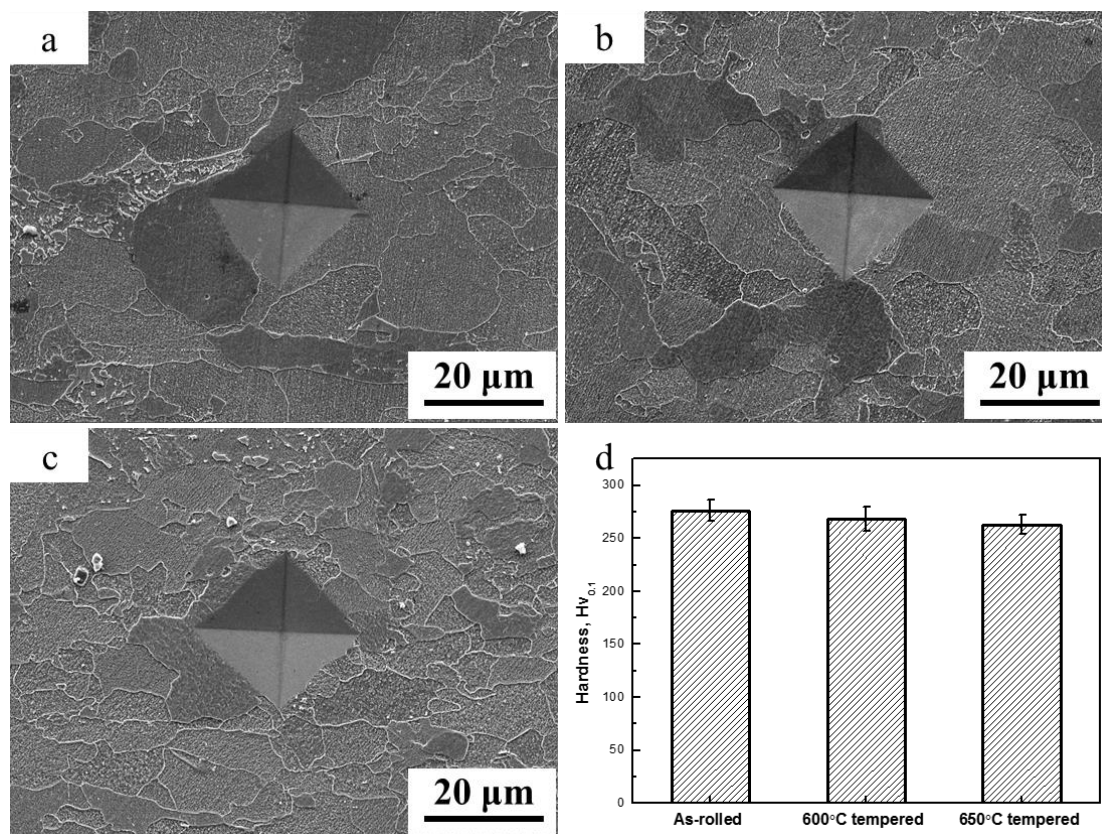


Figure 3. SEM images by secondary electron image mode showing a ferrite microstructure for samples after hot-rolling (a), holding at 600 °C (b) and 650 °C (c) for 3 h. (d) Microhardness plots for the studied steel.

3.3. Nanometer-Sized Precipitation

TEM was employed to study the nanometer-sized precipitation in ferrite before and after holding at high temperatures of 600 °C and 650 °C. The observed results for the hot-rolled sample are presented in Figure 4. Both random precipitates and interphase precipitates were obtained in ferrite after hot rolling and air cooling. It can be found that the row space of interphase precipitates was not uniform within the observed ferrite grain. As pointed out in Figure 4, the row spacing increased from ~24 nm to ~34 nm along the white dash arrow direction. Then, the precipitates existed in random distribution. EDS analysis indicated that these precipitates were (Ti, V)C complex carbides. A ledge mechanism proposed by Honeycombe and Mehl [22] is well accepted for interphase precipitation. During transformation from austenite (γ) to ferrite (α), a terrace γ/α plane with relatively low energy and a step γ/α plane with relatively high energy co-exist. The high-energy step γ/α plane moves too quickly to precipitate carbides during transformation. Yet, the low-energy terrace γ/α plane is immovable, such that carbides precipitate in the plane. When the electron beam is parallel to the precipitated terrace plane, row-arranged interphase precipitates are observed. The row spacing is related to the height of the step. Bhadeshia [23] suggested that the step height was proportional to the interface energy of the terrace plane and was inversely proportional to the driving force for ferrite transformation. This means reducing the driving force will increase the step height. In this study, carbon was enriched in austenite during ferrite growth. Liu et al. [24] revealed that carbon enrichment in austenite decreased the transformation temperature due to the reduction of driving force for ferrite transformation. This may be the reason for the increase in row spacing in the present work. Moreover, Chen et al. [25] suggested that $\gamma \rightarrow \alpha$ transformation becomes sluggish in the late ferrite transformation, the growth of carbides nucleated in the step plane was compatible with the

movement of the transformation front. Therefore, randomly dispersed carbide precipitation can be obtained in this instance.

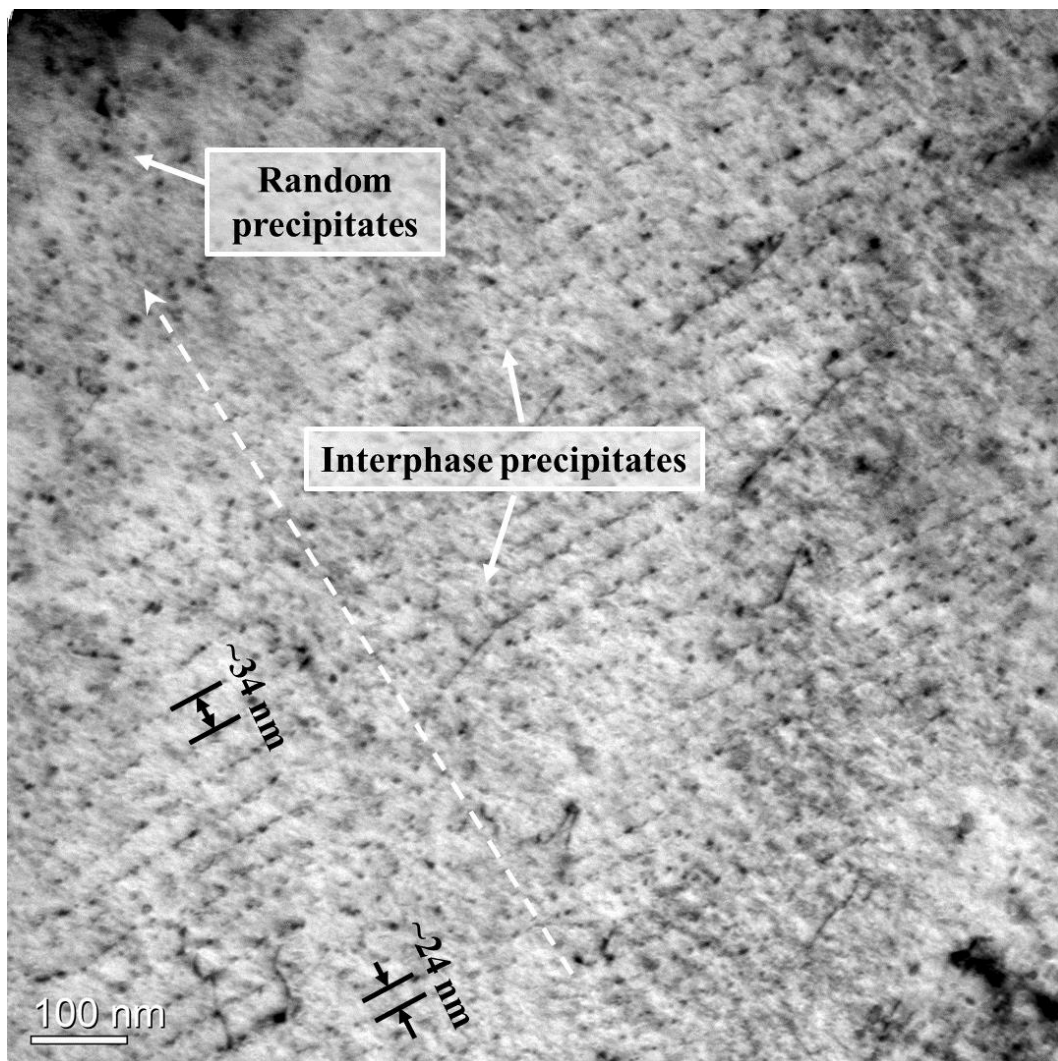


Figure 4. Bright-field TEM image obtained by FEI Tecnai F20 FE-TEM showing nanometer-sized precipitates in the hot-rolled sample.

Figure 5a,b present bright-field TEM images of nanometer-sized precipitates for samples after holding at 600 °C and 650 °C for 3 h, respectively. From Figure 5, interphase carbides were observed in both samples holding at 600 °C and 650 °C for 3 h, which is similar to those in the hot-rolled sample. In addition to interphase precipitated carbides, nanometer-sized carbides can be observed between interphase carbide rows, as pointed out by white arrows in Figure 5. To investigate the thermal stability of precipitation, the size of carbides for samples before and after holding at high temperatures was estimated statistically from hundreds of particles. As a matter of convenience, bright-field TEM images with random and dispersed carbides obtained by tilting the samples were used for the statistical estimation. The obtained results are plotted in Figure 6. It is clear that the complex (Ti, V)C precipitates have great resistance to growth when holding at high temperatures of 600 °C and 650 °C. The diameter of carbides in the hot-rolled sample was mainly in the range of 2–8 nm, and the average diameter was $\sim 6.1 \pm 2.7$ nm. After holding at 600 °C for 3 h, more than 80% of carbides had a diameter of 4–10 nm, and the average diameter increased slightly to $\sim 6.9 \pm 2.3$ nm. The diameter of carbides in the sample after holding at 650 °C for 3 h ranged from 4 to 15 nm with a peak at 8–10 nm. The average diameter

was further increased to $\sim 8.4 \pm 2.6$ nm. Dunlop and Honeycombe [26] studied the aging characteristics of (V, Ti)C dispersions in ferrite. Their results also indicated high resistance of (V, Ti)C precipitates to coarsening. The high stability of (V, Ti)C precipitates was suggested to be attributed to their high chemical bonding energy and low solubility in a ferritic matrix.

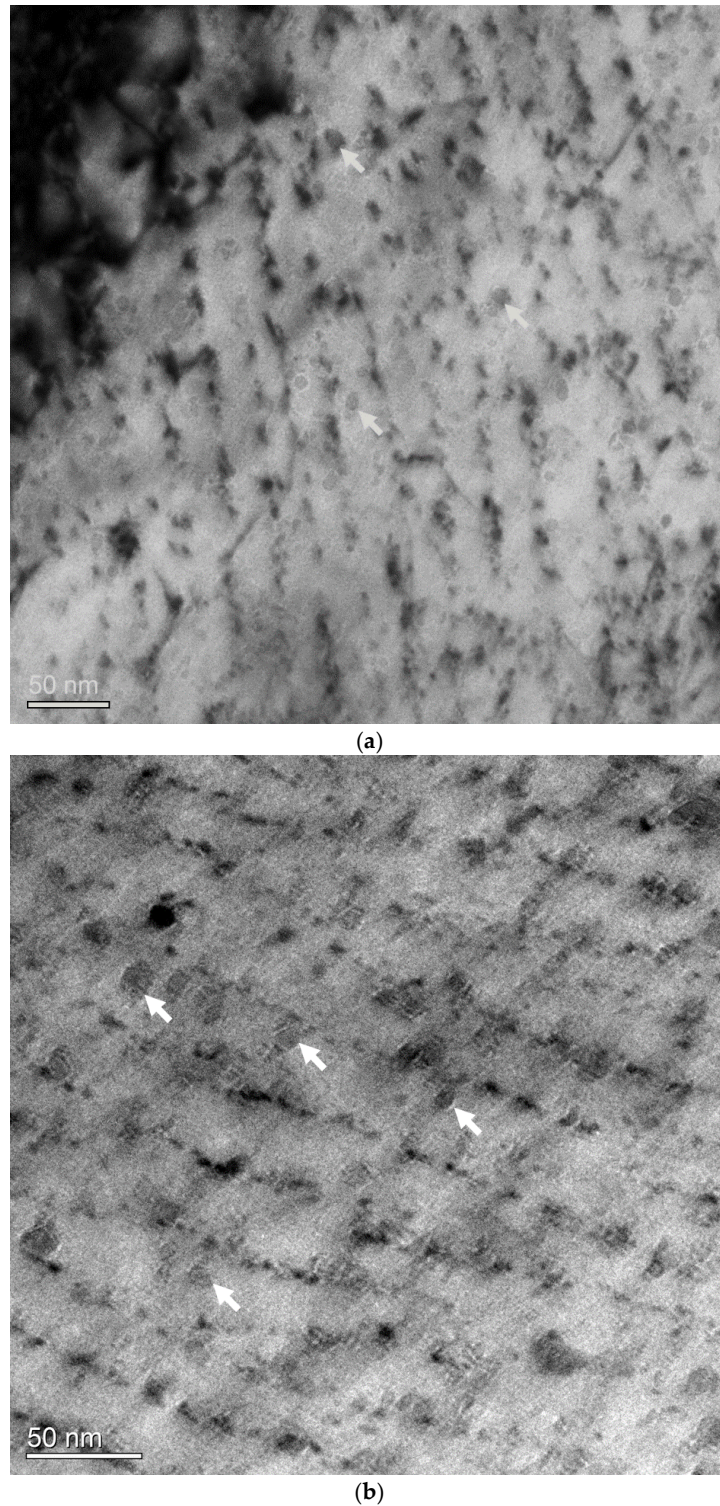


Figure 5. Bright-field TEM images showing nanometer-sized precipitates in samples after holding at 600 °C (a) and 650 °C (b) for 3 h, obtained by FEI Tecnai G20 TEM and FEI Tecnai F20 FE-TEM, respectively.

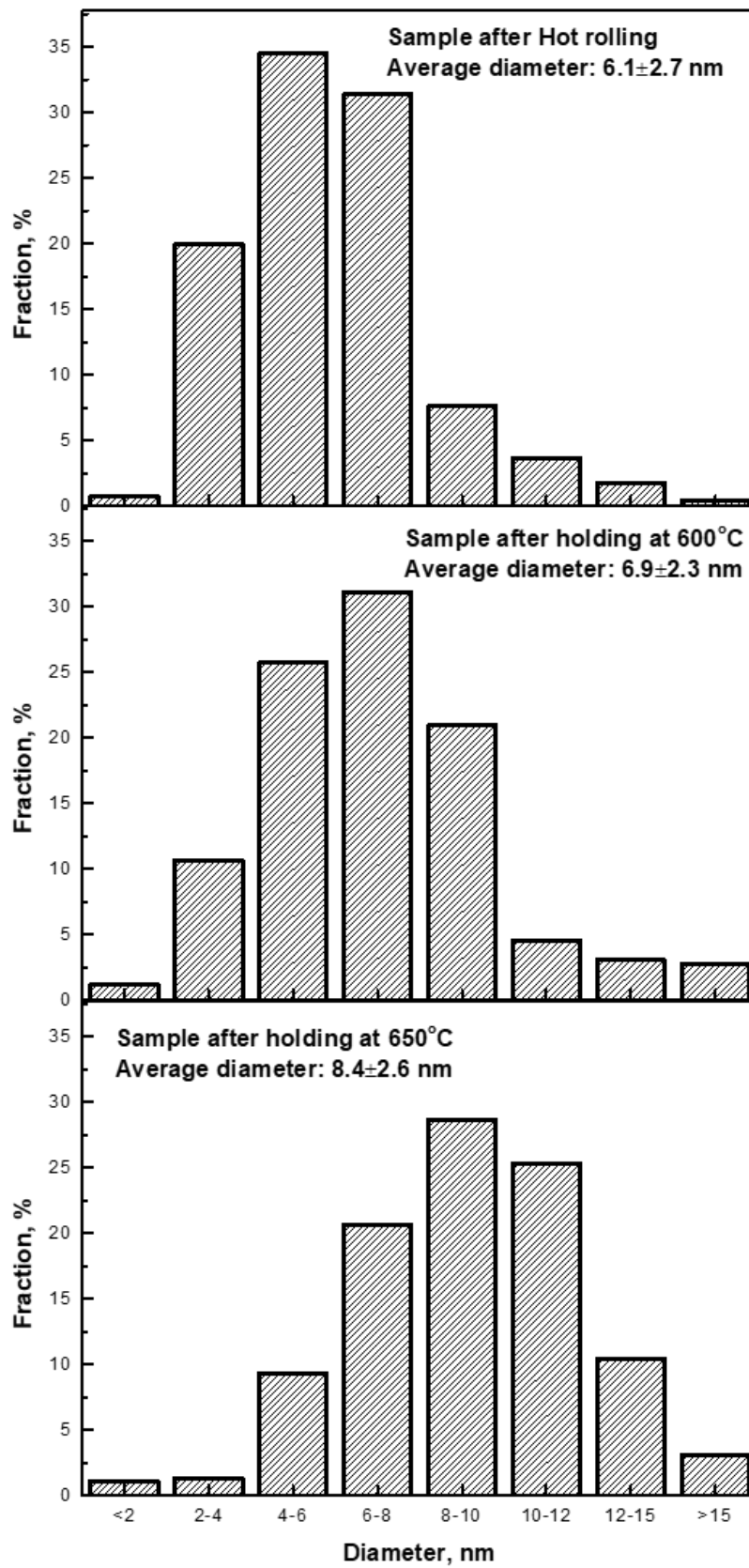


Figure 6. Size distributions of carbides for samples before and after holding at high temperatures.

3.4. Strengthening Mechanism

Generally, the yield strength of metals at room temperature is attributed to intrinsic friction stress, solid solute strengthening, grain boundary strengthening, dislocation strengthening, and precipitation hardening. For low carbon, low alloy ferritic steel, the strength contribution from precipitation hardening may be the greatest among all these strengthening mechanisms. The Ashby-Orowan model based on the mechanism of dislocations bypassing particles is normally accepted for evaluating precipitation strengthening provided by nanometer-sized hard (Ti, V)C carbides. Precipitation strengthening from MC-type carbides, according to the Ashby-Orowan model, is expressed by Equation (1) below [27,28].

$$\sigma_{ppt, Ashby-Orowan} = \frac{0.8MGb}{2\pi\sqrt{1-\nu}L_{MC}} \ln\left(\frac{x}{2b}\right) \text{ (MPa)} \quad (1)$$

$$L_{MC} = \sqrt{\frac{2}{3}} \left(\sqrt{\frac{\pi}{f}} - 2 \right) r_{MC} \text{ (m)} \quad (2)$$

$$x = 2\sqrt{\frac{2}{3}} r_{MC} \text{ (m)} \quad (3)$$

where M and ν is the Taylor factor and Poisson's ratio, taken as 2.75 and 0.29 for body-centered cubic metal with a random texture, respectively [29,30]. G is the shear modulus, b is the Burgers vector taken as 0.248 nm [31], r_{MC} is the average radius, and f is the volume fraction of MC-type carbides. It can be seen that the average diameter and volume fraction of carbides play determining roles in the strengthening effect. In the present work, the equilibrium volume fractions of MC-type carbides at different temperatures were calculated using commercial Thermo-Calc software with the TC-FE7 database [32,33]. The calculated results are plotted in Figure 7. The volume fraction of MC-type carbides increases when the temperature decreases, and reaches a maximum value of ~0.5% at 500 °C.

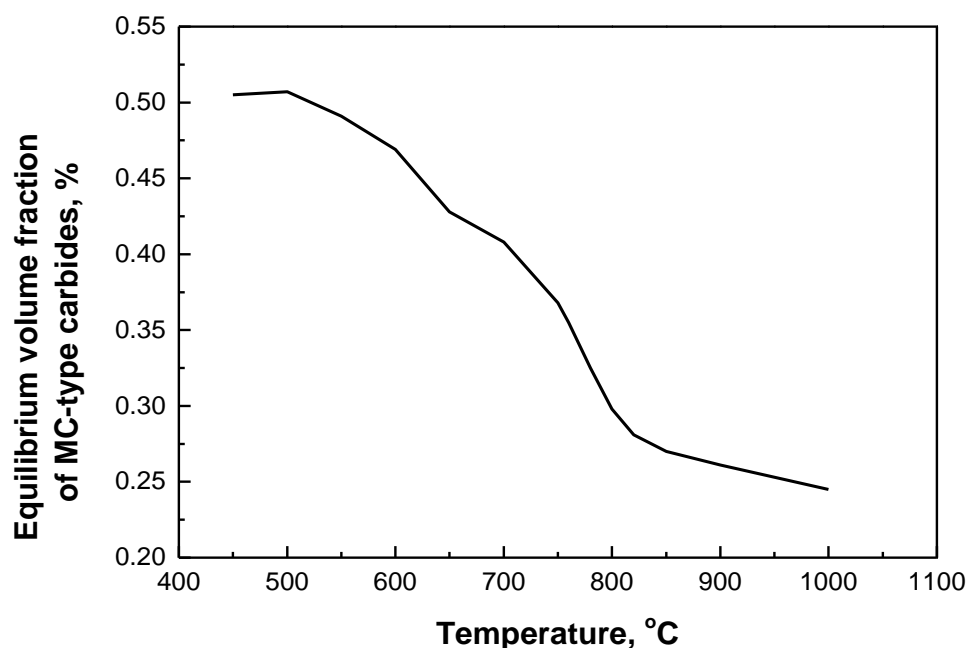


Figure 7. Equilibrium volume fraction of MC-type carbides vs. temperature plots calculated from commercial Thermo-Calc software with its TC-FE7 database.

At elevated temperatures, strength from precipitation strengthening is reduced due to the decrease in the shear modulus (G). The shear modulus (G) is related to Young's modulus (E) and Poisson's ratio (ν) by the following equation [30].

$$G = \frac{E}{2(1 + \nu)} \quad (4)$$

In the present work, the Young's modulus E of the studied steel at 600 °C and 650 °C was estimated by fitting the data of the elastic deformation stage from the stress-strain curves, as shown in Figure 8. The obtained Young's modulus E at room temperature and elevated temperatures of 600 °C and 650 °C were ~197 GPa, ~92 GPa, and ~69 GPa, respectively. Hence, the shear modulus (G) was ~76 GPa, ~36 GPa, and ~27 GPa for the studied steel at room temperature, at 600 °C, and at 650 °C, respectively. Assuming that the volume fraction (f) and the average diameter of MC-type carbides for the hot-rolled sample was respectively ~0.5% and 6.1 nm, the contribution from precipitation strengthening was estimated to be ~318 MPa to yield strength at room temperature, according to the Ashby-Orowan model. Given that the volume fraction of MC-type carbides was ~0.47% and ~0.43% from Figure 7 and the average diameter was 6.9 nm and 8.4 nm from Figure 6, the strength contribution from precipitation strengthening can be calculated to be ~133 MPa and ~84 MPa at 600 °C and 650 °C, respectively. It can be seen that the large volume fraction of nanometer-sized carbide precipitation provided a significant contribution to yield strength at room temperature and at an elevated temperature. The dramatic decrease in yield strength at 650 °C was attributed to the great loss in shear modulus at a higher temperature.

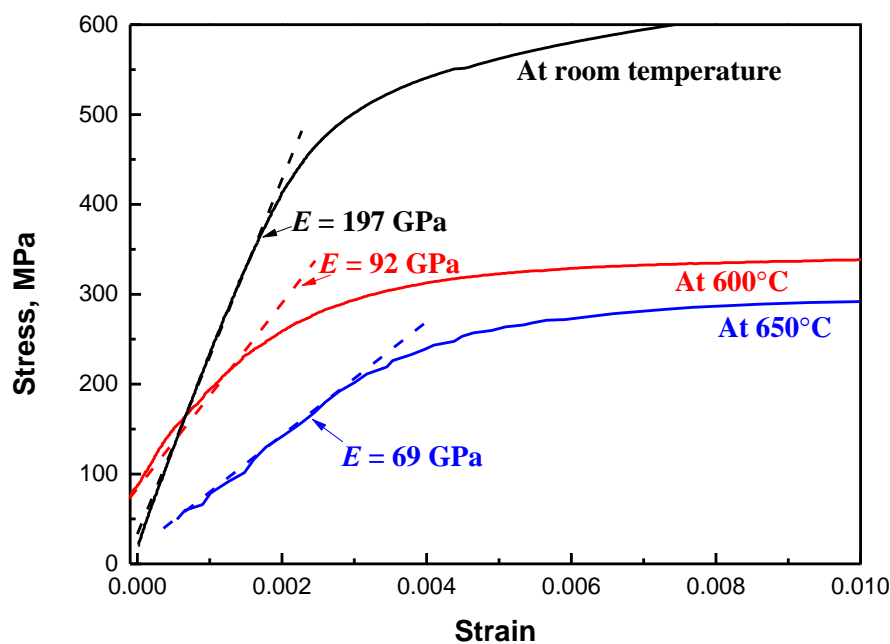


Figure 8. Fitted Young's modulus E at room temperature and elevated temperatures of 600 °C and 650 °C from stress-strain curves.

4. Conclusions

In this study, a multi-phase microstructure consisting of ferrite and a small fraction of bainite was obtained in a low-carbon low-alloy hot-rolled steel. Nanometer-sized precipitation and mechanical properties were investigated. The conclusions are summarized as follows.

- (1) Nanometer-sized interphase precipitates were obtained in ferritic matrix. The interphase precipitated carbides have been found to exhibit an average diameter of 6.1 ± 2.7 nm, with an average distance of ~24–34 nm by TEM observation. EDX results indicated that the precipitates were (Ti, V)C complex carbides.

- (2) The nanometer-sized precipitation exhibited high stability against tempering at high temperatures of 600 °C and 650 °C for 3 h. Average diameters of carbides were measured to be equal to $\sim 6.9 \pm 2.3$ nm and 8.4 ± 2.6 nm after annealing at high temperatures of 600 °C and 650 °C for 3 h, respectively.
- (3) Yield strength of 578 ± 20 MPa and tensile strength of 813 ± 25 MPa were achieved with high elongation of $25.0 \pm 0.5\%$ at room temperature. In addition, yield strength of 325 ± 13 MPa and 278 ± 4 MPa was achieved at elevated temperatures of 600 °C and 650 °C, respectively. Nanometer-sized precipitation contributed ~ 318 MPa to yield strength at room temperature, and the yield strength contributions decreased to ~ 133 MPa and ~ 84 MPa at 600 °C and 650 °C, respectively. The significant decrease of yield strength at 650 °C was attributed to the large decrease in the shear modulus.

Author Contributions: Writing—original draft preparation, Z.X.; investigation, Z.S., K.C., M.J. and Y.T.; methodology, X.W.; supervision, C.S.

Funding: The National Key R&D Program of China (No. 2017YFB0304700, 2017YFB0304701) and the National Natural Science Foundation of China (No. 51701012) funded this research.

Conflicts of Interest: The authors declare no conflict of interest.

References

1. Zhang, Z.Y.; Yong, Q.L.; Sun, X.J.; Li, Z.D.; Kang, J.Y.; Wang, G.D. Microstructure and mechanical properties of precipitation strengthened fire resistant steel containing high Nb and low Mo. *J. Iron Steel Res. Int.* **2015**, *22*, 337–343. [[CrossRef](#)]
2. Chijiwa, R.; Yoshida, Y.; Uemori, R.; Tamehiro, H.; Funato, K.; Horii, Y. Development and practical application of fire-resistant steel for buildings. *Nippon Steel Tech. Rep.* **1993**, *58*, 47–55.
3. Gross, C.T.; Isheim, D.; Vaynman, S.; Fine, M.E.; Chung, Y. Design and development of lightly alloyed ferritic fire-resistant structural steels. *Metall. Mater. Trans. A* **2019**, *50*, 209–219. [[CrossRef](#)]
4. Miyata, K.; Sawaragi, Y. Effect of Mo and W on the phase stability of precipitates in low Cr heat resistant steels. *ISIJ Int.* **2001**, *41*, 281–289. [[CrossRef](#)]
5. Mizutani, Y.; Ishibashi, K.; Yoshii, K.; Watanabe, Y.; Chihwa, R.; Yoshida, Y. 590MPa class of fire-resistant steel for building structural use. *Nippon Steel Tech. Rep.* **2004**, *90*, 38–44.
6. Wan, R.C.; Sun, F.; Zhang, L.T.; Shan, A.D. Effects of Mo on high-temperature strength of fire-resistant steel. *Mater. Des.* **2012**, *35*, 335–341. [[CrossRef](#)]
7. Wan, R.C.; Sun, F.; Zhang, L.T.; Shan, A.D. Effect of Mo addition on strength of fire-resistant steel at elevated temperature. *J. Mater. Eng. Perform.* **2014**, *23*, 2780–2786. [[CrossRef](#)]
8. Lee, W.B.; Hong, S.G.; Park, C.G.; Park, S.H. Carbide precipitation and high-temperature strength of hot-rolled high-strength, low-alloy steels containing Nb and Mo. *Metall. Mater. Trans. A* **2002**, *33*, 1689–1698. [[CrossRef](#)]
9. Wan, R.C.; Sun, F.; Zhang, L.T.; Shan, A.D. Development and study of high-strength low-Mo fire-resistant steel. *Mater. Des.* **2012**, *36*, 227–232. [[CrossRef](#)]
10. Assefpour-Dezfuly, M.; Hugaas, B.A.; Brownrigg, A. Fire resistant high strength low alloy steels. *Mater. Sci. Technol.* **1990**, *6*, 1210–1214. [[CrossRef](#)]
11. Funakawa, Y.; Shiozaki, T.; Tomita, K.; Yamamoto, T.; Maeda, E. Development of high strength hot-rolled sheet steel consisting of ferrite and nanometer-sized carbides. *ISIJ Int.* **2004**, *44*, 1945–1951. [[CrossRef](#)]
12. Khalid, F.A.; Edmonds, D.V. Interphase precipitation in microalloyed engineering steels and model alloy. *Mater. Sci. Technol.* **1993**, *9*, 384–396. [[CrossRef](#)]
13. Jang, J.H.; Heo, Y.U.; Lee, C.H.; Bhadeshia, H.K.D.H.; Suh, D.W. Interphase precipitation in Ti–Nb and Ti–Nb–Mo bearing steel. *Mater. Sci. Technol.* **2013**, *29*, 309–313. [[CrossRef](#)]
14. Miyamoto, G.; Hori, R.; Poorganji, B.; Furuhashi, T. Interphase precipitation of VC and resultant hardening in V-added medium carbon steels. *ISIJ Int.* **2011**, *51*, 1733–1739. [[CrossRef](#)]
15. Yen, H.W.; Chen, P.Y.; Huang, C.Y.; Yang, J.R. Interphase precipitation of nanometer-sized carbides in a titanium–molybdenum-bearing low-carbon steel. *Acta Mater.* **2011**, *59*, 6264–6274. [[CrossRef](#)]

16. Bu, F.Z.; Wang, X.M.; Yang, S.W.; Shang, C.J.; Misra, R.D.K. Contribution of interphase precipitation on yield strength in thermomechanically simulated Ti–Nb and Ti–Nb–Mo microalloyed steels. *Mater. Sci. Eng. A* **2015**, *620*, 22–29. [[CrossRef](#)]
17. Ferreira, D.; Alves, A.; Cruz Neto, R.; Martins, T.; Brandi, S. A new approach to simulate HSLA steel multipass welding through distributed point heat sources model. *Metals* **2018**, *8*, 951. [[CrossRef](#)]
18. Wang, S.T.; Yang, S.W.; Gao, K.W.; He, X.L. Corrosion resistance of low alloying weathering steels in environment containing chloride ion. *Trans. Mater. Heat Treat.* **2008**, *4*, 170–175.
19. Bhadeshia, H.; Honeycombe, R. *Steels: Microstructure and Properties*, 3rd ed.; Butterworth-Heinemann: Oxford, UK, 2006.
20. Chen, C.Y.; Chen, S.F.; Chen, C.C.; Yang, J.R. Control of precipitation morphology in the novel HSLA steel. *Mater. Sci. Eng. A* **2015**, *634*, 123–133.
21. Tsai, S.P.; Tsai, Y.T.; Chen, Y.W.; Yang, J.R.; Chen, C.Y.; Wang, Y.T.; Huang, C.Y. Precipitation behavior in bimodal ferrite grains in a low carbon Ti–V-bearing steel. *Scr. Mater.* **2018**, *143*, 103–107. [[CrossRef](#)]
22. Honeycombe, R.W.K.; Mehl, R.F. Transformation from austenite in alloy steels. *Metall. Trans. A* **1976**, *7*, 915–936. [[CrossRef](#)]
23. Bhadeshia, H.K.D.H. Diffusional transformations: A theory for the formation of superledges. *Phys. Stat. Sol. (a)* **1982**, *69*, 745–750. [[CrossRef](#)]
24. Liu, Z.Q.; Miyamoto, G.; Yang, Z.G.; Furuhashi, T. Direct measurement of carbon enrichment during austenite to ferrite transformation in hypoeutectoid Fe–2Mn–C alloys. *Acta Mater.* **2013**, *61*, 3120–3129. [[CrossRef](#)]
25. Chen, M.Y.; Yen, H.W.; Yang, J.R. The transition from interphase-precipitated carbides to fibrous carbides in a vanadium-containing medium-carbon steel. *Scr. Mater.* **2013**, *68*, 829–832. [[CrossRef](#)]
26. Dunlop, G.; Honeycombe, R. Ageing characteristics of VC, TiC, and (V, Ti) C dispersions in ferrite. *Metal Sci.* **1978**, *12*, 367–371. [[CrossRef](#)]
27. Ashby, M.F. *Physics of Strength and Plasticity*; The MIT Press: Cambridge, MA, USA, 1969.
28. Kelly, A.; Nicholson, R.B. Precipitation hardening. *Prog. Mater. Sci.* **1963**, *10*, 151–391.
29. Chin, G.Y.; Mammel, W.L. Computer solutions of the Taylor analysis for axisymmetric flow. *Trans. Metall. Soc. AIME* **1967**, *239*, 1400–1405.
30. Kaye, G.W.C.; Laby, T.H. *Tables of Physical and Chemical Constants and Some Mathematical Functions*, 14th ed.; Longman: London, UK, 1973.
31. Kamikawa, N.; Sato, K.; Miyamoto, G.; Murayama, M.; Sekido, N.; Tsuzaki, K.; Furuhashi, T. Stress–strain behavior of ferrite and bainite with nano-precipitation in low carbon steels. *Acta Mater.* **2015**, *83*, 383–396. [[CrossRef](#)]
32. Andersson, J.O.; Helander, T.; Höglund, L.; Shi, P.F.; Sundman, B. Thermo-Calc & DICTRA, computational tools for materials science. *Calphad* **2002**, *26*, 273–312.
33. Thermo-Calc Software. Available online: <http://www.thermocalc.com/> (accessed on 1 October 2019).

